Enhanced optical Kerr effect method for a detailed characterization of the third-order nonlinearity of two-dimensional materials applied to graphene

Evdokia Dremetsika and Pascal Kockaert*
Université libre de Bruxelles, OPERA-Photonics Group, 50 Avenue F.D. Roosevelt, CP 194/5 1050 Bruxelles, Belgium
(Received 20 September 2017; published 13 December 2017)

Using an enhanced optically heterodyned optical Kerr effect method and a theoretical description of the interactions between an optical beam, a single layer of graphene, and its substrate, we provide experimental answers to questions raised by theoretical models of graphene third-order nonlinear optical response. In particular, we measure separately the time response of the two main tensor components of the nonlinear susceptibility, we validate the assumption that the out-of-plane tensor components are small, and we quantify the optical impact of the substrate on the measured coefficients. Our method can be applied to other two-dimensional materials, as it relies mainly on the small ratio between the thickness and the wavelength.

DOI: 10.1103/PhysRevB.96.235422

I. INTRODUCTION

During the past decade, extensive research has been performed on graphene and other two-dimensional (2D) materials for applications in photonics and optoelectronics [1]. The third-order nonlinear optical response of graphene has been investigated by many groups both theoretically [2–8] and experimentally [9–15]. More recently, other 2D materials have also been studied [16,17]. Regarding the research trend combining graphene or 2D heterostructures with integrated photonics [1,18], characterization of 2D nonlinearities will play a key role in current and future progress in photonics.

The tensor nature of the nonlinear susceptibility of graphene has not yet been studied, although it is a parameter that could influence the observed nonlinearity, e.g., in waveguiding structures that can involve in- and out-of-plane components.

In this paper, we address the theoretical hypothesis [2–8,19] that the nonlinear optical response of graphene is limited to in-plane components. This apparently simple question is still open from an experimental point of view. It is indeed a long journey to provide an experimental answer by a direct measurement performed on a single-layer sample. The first reason is that a proper modeling of the interaction of an electromagnetic wave with a 2D material reveals that textbook expressions are incomplete, and that an extended theory should be used [20,21]. Secondly, as existing methods to probe 2D materials do not provide access to the real and imaginary parts of the third-order susceptibility tensor, it is also necessary to define a new experimental scheme.

The anisotropy induced by a pump beam on a graphene sample has been studied for different polarization angles between the pump and the probe [22,23], but there is no experimental work studying separately the two main tensor components used in the theory. Multiple reasons can probably explain this, including the very low signal provided by monolayer or few-layer graphene samples, the limited possibilities to probe various tensor components with Z-scan (which is a single-beam method), and the fact that only the magnitude of the fast component of $\chi^{(3)}$ is accessible in four-wave mixing experiments.

As explained in Ref. [14], the optically heterodyned optical Kerr effect method (OHD-OKE) [14,24] has many advantages over other widely used methods. In this paper, we implement an enhanced version called 2D-OHD-OKE, in which the sample is tilted, and linear polarization angles are tunable; and we provide the theoretical framework to extract tensor components from phase and amplitude jumps.

In Sec. II, we model the interactions of a plane wave with a graphene sheet and provide the expression of the 2D-OHD-OKE signal, taking into account new configurations that provide access to the real and/or imaginary parts of the tensor components of the nonlinear susceptibility. In Sec. III, we provide the temporal response of the tensor susceptibilities that can be accessed with our setup on a monolayer graphene on glass sample. In this way we achieve our goal, and we demonstrate that the measured out-of-plane components of the third-order nonlinear susceptibility tensor are negligible. We discuss the results and conclude on the use of 2D-OHD-OKE to access nonlinear optical parameters of any 2D material.

II. METHODS

In OHD-OKE, a pump and a probe pulse are focused on the sample (see [14], Fig. 1). The third-order nonlinearity of the sample is recorded by measuring the polarization changes induced by the pump on the weak probe pulse. As this polarization change is very small, optical heterodyning using a weak phase-shifted part of the probe is performed. Figure 1 shows the interaction of the two beams with the sample. We calculate the phase and amplitude changes by means of boundary conditions integrating the linear and nonlinear polarization response of the graphene surface.

A. Boundary conditions

Starting from the modeling of the sheet currents [20] at the planar interface between two semi-infinite media (a) and (b), we write each field $\vec{F}$ as

$$\vec{F} = \vec{F}_a(x,y,z)H(-z) + \vec{\mathcal{F}}(x,y)\delta(z) + \vec{F}_b(x,y,z)H(z), \quad (1)$$

with H the Heaviside step function and δ the Dirac distribution, where the surface field $\vec{\mathcal{F}}$ is located at $z = 0$ and varies in the (x,y) graphene plane. Inserting fields with these expressions

*pascal.kockaert@ulb.ac.be

in Maxwell's equations and collecting terms multiplying the same functions $H(z)$, $H(-z)$, $\delta(z)$, and $\delta'(z)$ provide elegantly the plane-wave solutions in the half-spaces defined by $z<0$ and $z>0$, as well as the boundary conditions at the interface. Assuming that media (a) and (b) are dielectric and isotropic, they are characterized by real refractive indices n_a and n_b. Writing the electric field $\vec{E}$, the displacement field $\vec{D}$, the polarization field $\vec{P}$, and the magnetic field $\vec{B}$ as in (1), we get the boundary conditions

$$\vec{B}_b-\vec{B}_a=-\hat{z}\times\mu_0\partial_t\vec{\mathcal{P}}, \tag{2}$$

$$\hat{z}\times(\vec{E}_b-\vec{E}_a)=-(\hat{z}\times\vec{\nabla})\mathcal{P}_z, \tag{3}$$

$$\hat{z}\cdot(\vec{D}_b-\vec{D}_a)=-\vec{\nabla}\cdot\vec{\mathcal{P}}, \tag{4}$$

which differ from those in Ref. [19] in that the polarization induced in the graphene sheet can have components along the z axis. This accounts for the extent of the orbitals on both sides of the graphene sheet. Starting from (2)–(4), and following the classical derivation of Fresnel coefficients (see Sec. 1.5 of Ref. [25]), we get the transfer matrix

$$E_t^{\parallel}=2\left(\frac{n_b}{n_a}+\frac{\cos\alpha_t}{\cos\alpha_i}\right)^{-1}\left[E_i^{\parallel}+i\frac{k_0}{2n_a}\frac{\mathcal{P}_x}{\varepsilon_0}-i\frac{k_0n_a}{2}\tan\alpha_i\frac{\mathcal{P}_z}{\varepsilon_0}\right], \tag{5}$$

$$E_t^{\perp}=2\left(1+\frac{n_b}{n_a}\frac{\cos\alpha_t}{\cos\alpha_i}\right)^{-1}\left[E_i^{\perp}+i\frac{k_0}{2n_a\cos\alpha_i}\frac{\mathcal{P}_y}{\varepsilon_0}\right], \tag{6}$$

where $\parallel$ and $\perp$ denote, respectively, the components parallel and orthogonal to the incidence plane of the incident and transmitted fields E_i and E_t, and α_i (α_t) is the angle between $\hat{z}$ and the incident (transmitted) wave vector. They verify the Snell-Descartes relation $n_a\sin\alpha_i=n_b\sin\alpha_t$. For later use, we define the coefficients M,N,P,Q,R so that

$$\begin{bmatrix}E_t^{\parallel}\\E_t^{\perp}\end{bmatrix}=\begin{bmatrix}P&0\\0&M\end{bmatrix}\begin{bmatrix}E_i^{\parallel}\\E_i^{\perp}\end{bmatrix}+\frac{1}{\varepsilon_0}\begin{bmatrix}Q&0&R\\0&N&0\end{bmatrix}\begin{bmatrix}\mathcal{P}_x\\\mathcal{P}_y\\\mathcal{P}_z\end{bmatrix}, \tag{7}$$

where the coefficients Q, N, and R are in the order of k_0.

B. Linear material response

The main difference between a model of graphene using bulk or surface parameters appears in the constitutive relations. Indeed, in the bulk approach, the polarization of the medium is calculated with respect to the field transmitted in the graphene using (5) and (6), with $n_b=n_g$ the refractive index of graphene and $\mathcal{P}=0$. In the surface approach, we should consider the total electric field surrounding the surface sheet, as explained in Refs. [21] and [26]. In what follows, we calculate this field as the symmetric combination [21] of the incident $(\vec{E}_i)$, reflected $(\vec{E}_r)$, and transmitted $(\vec{E}_t)$ field in the graphene plane. Assuming that the contribution of the graphene susceptibility is a small perturbation of the total field, we set $\mathcal{P}=0$ to calculate this symmetric surface field $\vec{E}^{(s)}=[\vec{E}_i+\vec{E}_r+\vec{E}_t]/2$ in the axes of the sample (see Fig. 1),

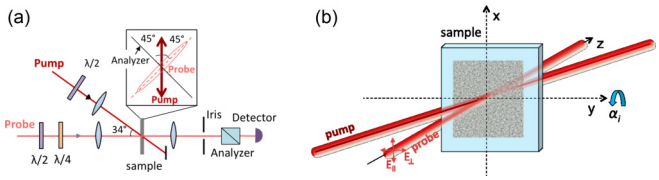

FIG. 1. (a) Interaction of the pump-and-probe beams with the sample. Half- and quarter-wave plates are denoted, respectively, by $\lambda/2$ and $\lambda/4$. Iris denotes an iris diaphragm. (b) The pump-and-probe beams define the horizontal plane that intersects the sample along the y axis. Sample tilt around $\hat{y}$ is denoted by α_i.

$$\begin{bmatrix}E_x^{(s)}\\E_y^{(s)}\\E_z^{(s)}\end{bmatrix}=\begin{bmatrix}\cos\alpha_t&0\\0&1\\-\sin\alpha_t\left(1+n_b^2/n_a^2\right)/2&0\end{bmatrix}\begin{bmatrix}E_t^{\parallel}\\E_t^{\perp}\end{bmatrix}, \tag{8}$$

so that we can finally calculate the contribution of the graphene surface to the transmitted field, combining

$$\mathcal{P}_i=\varepsilon_0\sum_{j=x,y,z}\chi_{ij}\otimes E_j^{(s)}\ (i=x,y,z) \tag{9}$$

with (8), (5), and (6). In (9), $\otimes$ denotes the convolution product on time. Note that due to (1), χ_{ij} is a surface quantity that could be linked to the volume quantity χ_{ij}^v using $\chi_{ij}=d\chi_{ij}^v$, where $d\approx 0.33$ nm is taken as the distance between two graphene sheets. For χ_{ij}^v in the order of unity, $k_0\chi_{ij}\sim k_0d<10^{-3}$ in the visible and infrared regions.

This theory is valid for linear interactions. In the following section, we show that it can apply equally to the pump-probe geometry of Fig. 1 when we are interested in the Kerr effect and two-photon absorption.

C. Nonlinear interaction

Most theoretical papers on graphene use the conductivity σ_{ij} rather than the susceptibility χ_{ij}. In what follows, we will consider the surface polarization that is linked to the surface current $\vec{\mathcal{J}}=\partial_t\vec{\mathcal{P}}$, so that $\sigma_{ij}(t)=\varepsilon_0\partial_t\chi_{ij}(t)$, or equivalently in the spectral domain $\tilde{\sigma}_{ij}(\omega)=-i\varepsilon_0\omega\tilde{\chi}_{ij}(\omega)$.

To allow for a complete description of the material properties in the pump-probe geometry of Fig. 1, we model the third-order current density using

$$\mathcal{P}_i^{(3)}(t)=\varepsilon_0\sum_{j,k,l=x,y,z}\chi_{ijkl}^{(3)}\overset{1}{\otimes}E_j^{(s)}\overset{2}{\otimes}E_k^{(s)}\overset{3}{\otimes}E_l^{(s)}, \tag{10}$$

where $\overset{n}{\otimes}$ denotes the convolution on the nth variable of $\chi_{ijkl}^{(3)}(t_1,t_2,t_3)$, and the electric-field components $E_l^{(s)}$ can be written as the sum of paraxial pump (p) and probe (b) beams,

$$\begin{aligned}E_l^{(s)}&=E_l^{p,(s)}+E_l^{b,(s)}+\text{(c.c.)}\\&=\left[A_l^pe^{i\vec{k}_p\vec{r}}+A_l^be^{i\vec{k}_b\vec{r}}\right]+\text{(c.c.)},\end{aligned} \tag{11}$$

where (c.c.) denotes the complex conjugate.

In the setup depicted in Fig. 1, the iris selects the output component collinear with the probe beam. Introducing (11) in (10) shows that these components appear in terms

containing one factor $E^b_\cdot$, and either the pair $(E^{b,(s)}_\cdot, E^{b,(s)*}_\cdot)$ or $(E^{p,(s)}_\cdot, E^{p,(s)*}_\cdot)$, where $\cdot$ denotes any index. Taking into account that the signal beam is very weak in comparison with the pump beam, we get the spatially filtered contribution

$$\mathcal{P}^{(3)}_{\vec{k}_s,i}(t) = 6\,\varepsilon_0 \sum_{j,k,l=x,y,z} \chi^{(3)}_{ijkl} \overset{1}{\otimes} E^{b,(s)}_j \overset{2}{\otimes} E^{p,(s)\,*}_k \overset{3}{\otimes} E^{p,(s)}_l, \tag{12}$$

in which the leading 6 comes from the intrinsic symmetries of the susceptibilities [27]. From (12) we define a pseudolinear susceptibility independent of the absolute phase of E^p,

$$\chi^{\mathrm{NL}}_{ij}(t_1) = 6 \sum_{k,l=x,y,z} \chi^{(3)}_{ijkl}(t_1,t_2,t_3) \overset{2}{\otimes} E^{p,(s)\,*}_k \overset{3}{\otimes} E^{p,(s)}_l, \tag{13}$$

that depends on the pump signal shape and intensity, so that

$$\mathcal{P}_{\vec{k}_s,i} = \varepsilon_0 \sum_{j=x,y,z} \left[\chi^{(1)}_{ij} + \chi^{\mathrm{NL}}_{ij}\right] \otimes E^{b,(s)}_j = \varepsilon_0 \sum_{j=x,y,z} \chi_{ij} \otimes E^{b,(s)}_j, \tag{14}$$

which defines an effective first-order susceptibility for $E^{b,(s)}$.

D. Optical Kerr effect

Combining (9), (8), (5), (6), and (14), we find a transfer matrix between the incident and transmitted polarization components,

$$\begin{bmatrix} E^{\parallel}_t \\ E^{\perp}_t \end{bmatrix} = \mathcal{M} \begin{bmatrix} E^{\parallel}_i \\ E^{\perp}_i \end{bmatrix} = \begin{bmatrix} A & B \\ C & D \end{bmatrix} \begin{bmatrix} E^{\parallel}_i \\ E^{\perp}_i \end{bmatrix}, \tag{15}$$

where

$$A = P + PQ\chi_{x\parallel} + PR\chi_{z\parallel}, \tag{16}$$

$$B = MQ\chi_{xy} + MR\chi_{zy}, \tag{17}$$

$$C = PN\chi_{y\parallel}, \tag{18}$$

$$D = M + MN\chi_{yy}, \tag{19}$$

$$\chi_{i\parallel} = \cos\alpha_t \chi_{ix} - \sin\alpha_t \left(1 + n_b^2/n_a^2\right)/2\, \chi_{iz}. \tag{20}$$

Measurement of the effects induced by the pump beam on the probe could be performed as follows. First, we switch the pump off, which defines the transfer matrix $\mathcal{M}_0$, and we set a normalized probe polarization state $I_0 = (E^{\parallel}_i, E^{\perp}_i)^t/E_i$, which defines the normalized output state $T_0 = \mathcal{M}_0 I_0/E_t$. Then we tune the output analyzer to get a zero transmitted signal. This is equivalent to projecting on the state $T_\perp = (-T_0^\perp, T_0^\parallel)^\dagger$ orthogonal to T_0. Finally, we switch the pump on, which induces a nonlinear change $\delta\mathcal{M} = \mathcal{M} - \mathcal{M}_0$ on the transfer matrix, and we detect the power change at the output, given by

$$|E_{\mathrm{out}}|^2 = |T_\perp^\dagger \delta\mathcal{M} I_0|^2 \left|E^b_i\right|^2. \tag{21}$$

This signal is very weak as it is proportional to $\delta\mathcal{M}^2 \sim (k_0 d)^2 < 10^{-6}$, and it does not provide the sign of $\delta\mathcal{M}$. To improve this, optical heterodyning is performed.

E. Optical heterodyning

We make a slight change to the input conditions on the quarter-wave plate in Fig. 1, or we modify the analyzer angle, so that the input polarization state becomes $I_1 = (I_0 + i\theta I_\perp)/\sqrt{1+|\theta|^2}$ or the projection state becomes $T_1 = (T_\perp + \eta T_0)/\sqrt{1+|\eta|^2}$, where the terms proportional to θ and η correspond to the local oscillator field [14,24]. The measured output field is therefore

$$|E_{\mathrm{out}}|^2 = |T_1^\dagger(\mathcal{M}_0 + \delta\mathcal{M})I_1|^2 \left|E^b_i\right|^2. \tag{22}$$

To isolate the weak nonlinear signal from the background, both the pump and probe beams are modulated at low frequencies Ω_p and Ω_b by means of a chopper [28], and the signal power is measured, with a lock-in amplifier at $\Omega_{bp} = \Omega_p + \Omega_b$, to first order in $\delta\mathcal{M}$. The 2D-OHD-OKE signal is

$$S(\theta,\eta) = 2\,\mathrm{Re}[(T_1^\dagger \mathcal{M}_0 I_1)^*(T_1^\dagger \delta\mathcal{M} I_1)] \left|E^b_i\right|^2. \tag{23}$$

In bulk OHD-OKE, $(\delta\mathcal{M})^2$ cannot be neglected as $k_0 d \geqslant 1$, which leads to an additional "homodyne" signal. The incident electric fields in medium (a) can be calculated from the incident power P and the effective beam area πw_0^2 on the sample, using $P^b = 2\pi w_{0b}^2 \varepsilon_0 n_a c |E^b_i|^2$, and the same for P^p.

F. In-plane 2D-OHD-OKE

As an example, we consider the in-plane 2D-OHD-OKE configuration depicted in Fig. 1 and used in Ref. [14]. The heterodyne parameters used to measure the real part of the nonlinear response are $\eta = 0$ and $\theta \neq 0$, and the refractive indices are $n_a = 1$ and $n_b = 1.5$ for a glass substrate. As the sample is not tilted, $\alpha_i = 0 = \alpha_t$. We therefore have $P = M = 2/(1+n_b)$, $N = Q = ik_0/(1+n_b)$, and $R = 0$. From (20), we have $\chi_{i\parallel} = \chi_{ix}$, and therefore

$$\mathcal{M} = 2 \begin{bmatrix} (1+n_b) + ik_0\chi_{xx} & ik_0\chi_{xy} \\ ik_0\chi_{yx} & (1+n_b) + ik_0\chi_{yy} \end{bmatrix} \Big/ (1+n_b)^2. \tag{24}$$

Pump-and-probe polarizations are depicted in the inset of Fig. 1. The input state is defined by $I_0 = (1,1)^t/\sqrt{2}$. When the pump is switched off, $\chi_{ij} = \chi^{(1)}_{ij} = \chi_g \delta_{ij}$ due to the sixth-order symmetry of graphene, so that $\mathcal{M}_0$ is the identity matrix multiplied by $2[1 + ik_0\chi_g/(1+n_b)]/(1+n_b)$, which implies $T_0 = I_0$ and $T_1 = T_\perp = I_\perp = (-1,1)^t/\sqrt{2}$. As $\mathcal{M}_0$ will be multiplied by a first-order term in $k_0 d$, we can ignore the term proportional to $k_0\chi_g$, so that $T_1^\dagger \mathcal{M}_0 I_1 = 2i\theta/(1+n_b)$.

To evaluate $\delta\mathcal{M}$, we calculate the pump field, which is vertically polarized, orthogonal to its horizontal incidence plane. Therefore, the symmetric surface field is given by $E^{p,\perp}_t$ according to (8). As this beam makes an angle α^p_i with $\hat{z}$, using (6) we get $E^{p,(s)}_x = 2E^p_i/(1 + n_b \cos\alpha^p_t/\cos\alpha^p_i)$, with $\alpha^p_t = \sin^{-1}(\sin\alpha^p_i/n_b)$. Using (13) and the symmetries of the third-order susceptibility tensor, we get

$$\delta\mathcal{M} = \frac{12ik_0}{(1+n_b)^2} \begin{bmatrix} \chi_{xxxx} & 0 \\ 0 & \chi_{yyxx} \end{bmatrix} \left|E^{p,(s)}_x\right|^2, \tag{25}$$

$$S(\theta,0) = S_0 \mathrm{Re}[\theta^*(\chi_{yyxx} - \chi_{xxxx}) + i|\theta|^2(\chi_{xxxx} + \chi_{yyxx})],$$

$$S_0 = \frac{96k_0 \left|E^p_i E^b_i\right|^2}{(1+|\theta|^2)(1+n_b)^3 \left(1 + n_b \cos\alpha^p_t/\cos\alpha^p_i\right)^2}, \tag{26}$$

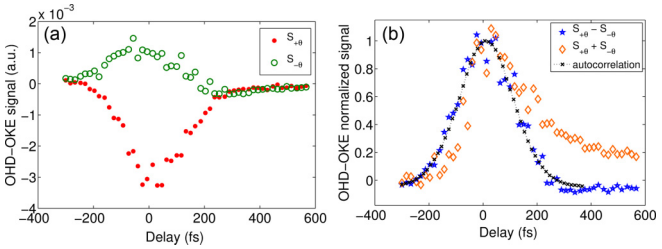

FIG. 2. Experimental results: (a) 2D-OHD-OKE signal of graphene at positive and negative heterodyne angle. (b) Normalized difference and sum of 2D-OHD-OKE signals from (a) compared with the pulse autocorrelation obtained by the OHD-OKE signal from the silicon reference sample.

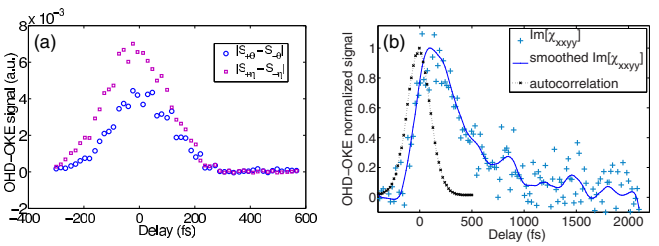

FIG. 3. Experimental results: (a) comparison between $|S^{\theta}_{\rm dif}|$ and $|S^{\eta}_{\rm dif}|$; (b) normalized $S^{\theta}_{\rm sum}$ for parallel pump-and-probe polarizations, providing $\mathrm{Im}(\chi_{xxyy})$ compared with the autocorrelation. Smoothed data (Savitzky-Golay) are provided as a guide for the eye.

where, for the sake of simplicity, we write $\chi_{ijkl} = \chi^{(3)}_{ijkl}$. Taking $S(\theta,0) - S(-\theta,0)$, we get access to $\mathrm{Re}(\chi_{xxxx} - \chi_{yyxx}) = \mathrm{Re}(\chi_{xyxy} + \chi_{xyyx})$, where we have used symmetry relations.

Using (26) and the data from Ref. [14], we calculate $\mathrm{Re}(\chi_{xyxy} + \chi_{xyyx}) = -200\ \mathrm{nm}^3/\mathrm{V}^2$.

III. EXPERIMENTAL RESULTS

In our experiments, we used a monolayer graphene film on glass from Graphene Laboratories, Inc.; the film was grown by catalyzed chemical vapor deposition (CVD). We verified that the glass substrate does not present a nonlinear response.

Our experimental setup is based on that depicted in Ref. [14], with the modifications appearing in Fig. 1. The 180-fs pulses at 1600 nm were derived from an optical parametric oscillator (OPO), pumped by a Ti:sapphire laser, with a repetition rate of 82 MHz. The pump-probe power ratio is tuned around 15:1. The pump-and-probe beams are spatially overlapped on the sample and focused down to a beam waist of $w_p \approx 20\ \mu$m and $w_b \approx 15\ \mu$m, respectively. The pump intensity is set around $5 \times 10^{12}\ \mathrm{W/m^2}$, which is far below the damage threshold of graphene [29]. The effective interaction length was $L \approx 100\ \mu$m. The heterodyne parameters were either $\theta = \pm\tan 4^\circ$, $\eta = 0$ or $\eta = \pm\tan 4^\circ$, $\theta = 0$. The angle between the pump and the probe beam is 34°. For the out-of-plane measurements, the sample was rotated with a precision rotation mount. As in Ref. [14], we used a silicon reference sample.

A. Temporal response of the tensor components

Starting with the configuration described in Sec. II F, we recorded the temporal response of the 2D-OHD-OKE signal shown in Fig. 2(a). At long delay, both signals are equal, which is explained by studying the different tensor components, namely by taking the difference and the sum of the signals $S(\theta,0)$ and $S(-\theta,0)$ from (26). As shown in Fig. 2(b), the first signal, $S^{\theta}_{\rm dif} \propto \theta\,\mathrm{Re}(\chi_{xyxy} + \chi_{xyyx})$, which is purely due to induced birefringence, has a fast response. This is indeed demonstrated by the perfect fit with the autocorrelation trace of the input pulses, which implies a relaxation time shorter than the 180-fs pulse duration. The second signal, $S^{\theta}_{\rm sum} \propto \theta^2\,\mathrm{Im}(\chi_{xyxy} + \chi_{xyyx} + 2\chi_{xxyy})$, appears due to the nonlinear absorption of the local oscillator field and therefore is negligible for materials with weak nonlinear absorption. Here this signal is important, and it presents a completely different behavior from the birefringent signal, with a picosecond relaxation time characteristic of graphene [30].

Next, we studied induced dichroism, which corresponds to the imaginary part of the nonlinearity, similarly to the birefringence, by considering $S(0,\eta)$ and $S(0,-\eta)$ [see Fig. 3(a)]. The induced dichroism $S^{\eta}_{\rm dif} \propto \eta\,\mathrm{Im}(\chi_{xyxy} + \chi_{xyyx})$ is also characterized by a fast relaxation, which is in agreement with the conclusion of Mittendorf *et al.* [22] that the anisotropic distribution of photoexcited carriers in graphene has a fast relaxation time of 150 fs. This anisotropic distribution is actually the microscopic origin of the induced dichroism or birefringence. The expression (and the observed behavior) of $S^{\eta}_{\rm sum}$ is the same as $S^{\theta}_{\rm sum}$. The ratio from the nonlinear dichroic losses to the nonlinear birefringence is evaluated to $S^{\eta}_{\rm dif}/S^{\theta}_{\rm dif} \approx 1.6$, which provides $\mathrm{Im}(\chi_{xyxy} + \chi_{xyyx}) \approx -320\ \mathrm{nm}^3/\mathrm{V}^2$ at zero pump-probe delay.

We compared the in-plane OHD-OKE data of graphene and silicon, as we did in Ref. [14], for the real part of the nonlinearity. We verified that the two-photon absorption coefficient of silicon is in agreement with published values. As for the refractive part [14], the signals of graphene and silicon presented opposite signs, which is not surprising since it is well known that graphene is a saturable absorber. Saturable absorption does not scale linearly with the input intensity, so the measured $\mathrm{Im}(\chi_{xyxy} + \chi_{xyyx})$ should decrease with increasing intensity. This was confirmed experimentally.

Finally, the imaginary part of χ_{xxyy} was studied separately by taking measurements in a different configuration, in which the input pump-and-probe polarizations are parallel. In this case, we get $S^{\theta}_{\rm sum} \propto \theta^2\,\mathrm{Im}(\chi_{xxyy})$, which is shown in Fig. 3(b). We infer that the relaxation time of $\mathrm{Im}(\chi_{xxyy})$ is around 1 ps. By comparing the magnitude of the signals, we find $\mathrm{Im}(\chi_{xxyy}) \approx 1.7\,\mathrm{Im}(\chi_{xyxy} + \chi_{xyyx})$. We note that $\mathrm{Re}(\chi_{xxyy})$ is not accessible with simple experimental configurations, but it has probably the same temporal dependence as $\mathrm{Im}(\chi_{xxyy})$. At zero pump-probe delay, we find $\mathrm{Im}(\chi_{xxyy}) \approx -540\ \mathrm{nm}^3/\mathrm{V}^2$.

B. Out-of-plane tensor components

To measure the out-of-plane tensor components, we tilt the sample around the horizontal axis so that $\alpha_i = 30^\circ$, and we calculate the coefficients C_{ijkl} appearing in $S(\theta,0) - S(-\theta,0) = S_1\mathrm{Re}(2\theta^* \sum_{ijkl=x,y,z} C_{ijkl}\chi_{ijkl})$. When the input polarization of the probe beam is set vertical or horizontal, only

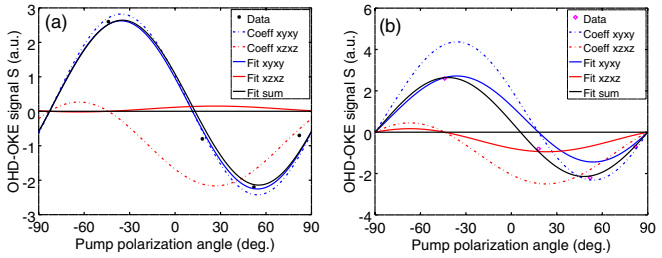

FIG. 4. Experimental data and fitting of the odd part of the 2D-OHD-OKE signal for a vertical input polarization of the probe (x axis). The linear pump polarization is continuously set from vertical ($-90°$) to horizontal ($0°$) and vertical ($90°$). C_{xyxy} and C_{xzxz} denote, respectively, the coefficients of the real parts of $\chi_{xyxy} + \chi_{xyyx}$ and $\chi_{xzxz} + \chi_{xzzx}$. Data are fitted to these curves: black, total fit; blue, $xyxy$ component; red, $xzxz$ component. Coefficients C_{xyxy} and C_{xzxz} are calculated using (a) the symmetric surface field, and (b) without taking the field in the substrate into account.

four coefficients appear in $S(\theta,0) - S(-\theta,0)$: $C_{xyxy} = C_{xyyx}$ and $C_{xzxz} = C_{xzzx}$ or $C_{zxzx} = C_{zxxz}$, respectively. With the probe polarized vertically, their variation with the polarization of the pump beam is shown in Fig. 4 (dotted-dashed lines). Experimental data appear as black dots. In panel (a) the symmetric surface field is used, as explained in Sec. II B, while in panel (b) the expressions for bulk materials are used. The relative values of $\mathrm{Re}(\chi_{xyxy} + \chi_{xyyx})$ and $\mathrm{Re}(\chi_{xzxz} + \chi_{xzzx})$ are obtained by fitting the experimental data. In Fig. 4, the black curve shows the fitted curve while the blue and red curves show the contributions of the two sets of susceptibilities to the total curve. In panel (a) we see that the contribution $xzxz$ to the fit is very weak, and it is not needed to explain the experimental data, as its amplitude is in the order of the experimental error. Setting $\eta = \pm\tan 4°$ and $\theta = 0$, $S(0,\eta) - S(0,-\eta)$ provides the ratio of the imaginary parts of the same components, which demonstrates that $|\chi_{xzxz} + \chi_{xzzx}|/|\chi_{xyxy} + \chi_{xyyx}| < 0.1$. Using a second set of experimental data, with the probe beam polarized horizontally, we reach similar conclusions for the real and imaginary parts of $\chi_{zxzx} + \chi_{zxxz}$. These results validate the theoretical assumptions that χ_{xzxz}, χ_{xzzx}, χ_{zxzx}, and χ_{zxxz} are negligible [5], with a magnitude that does not exceed 20 $\mathrm{nm}^3/\mathrm{V}^2$. Figure 4(b) shows that the use of a bulk theory neglecting the substrate provides a ratio around 0.5, which would lead to an opposite conclusion.

IV. DISCUSSION

A. In-plane components

To compare our values of the in-plane components with other values from the literature that are mostly reported as volume susceptibilities or as an effective nonlinear refractive index, we provide the appropriate conversions in Table I.

Comparison of the effective nonlinear refractive index with the earlier values from Z-scan [11,12] was provided in a previous work [14]. More recent reported values [13,31] are in good agreement, in sign and magnitude, with those already published values. It should be noted that Z-scan probes the nonlinearity related to $\mathrm{Re}(\chi_{xxxx})$, so that we do not expect an exact match of the results. This is also true for results from four-wave-mixing (FWM) experiments. Because we have not measured $\mathrm{Re}(\chi_{xxyy})$, we estimate the magnitude of the volume susceptibility $|\chi_v^{(3)}|$ either by neglecting the χ_{xxyy} component or by assuming that $\mathrm{Re}(\chi_{xxyy})$ is on the order of $\mathrm{Re}(\chi_{xyxy} + \chi_{xyyx})$. In both cases, we get an absolute value in the order of 10^{-7} esu, which is in agreement with the value from Ref. [9].

TABLE I. Estimated parameters of the third-order optical nonlinearity from 2D-OHD-OKE. The real part of the complex nonlinear index n_{2c} corresponds to the effective nonlinear refractive index measured in a previous work [14]. Conversion between this value and the surface susceptibility is performed using $k_0 dn_2 P^p/(\pi w_{0p}^2)$ for the phase shift. All the parameters correspond to the surface components $\chi_{xyxy} + \chi_{xyyx}$. They are obtained with a pump intensity around 5×10^{12} $\mathrm{W/m^2}$. The real (imaginary) part of $\sigma^{(3)}$ is calculated from the imaginary (real) part of $\chi^{(3)}$.

	n_{2c}	$\chi_s^{(3)}$	$\chi_v^{(3)}$	$\chi_v^{(3)}$	$\sigma^{(3)}$
Units	$\mu\mathrm{m}^2/\mathrm{W}$	$\mathrm{nm}^3/\mathrm{V}^2$	$\mathrm{nm}^2/\mathrm{V}^2$	esu	$\mathrm{Am}^2/\mathrm{V}^3$
Real	-0.1	-200	-600	-0.4×10^{-7}	-3.3×10^{-21}
Imag.	-0.16	-320	-960	-0.65×10^{-7}	2.1×10^{-21}

To compare our results with theoretical values, we need to estimate the doping level of our graphene sample. Graphene deposited on glass or silicon substrates is low p-doped, as shown, for example, in Ref. [15], where the chemical potential is evaluated between -0.3 and -0.2 eV. At those doping levels and the wavelength used in our experiments (1600 nm, or $\hbar\omega \approx 0.8$ eV), the nonlinear conductivity in Ref. [4] diverges. Assuming higher doping levels, so that $\hbar\omega/|\mu| < 2$, Cheng and co-workers estimated a nonlinear refractive index two orders of magnitude lower than our value. In a later theoretical work [5], the same authors added phenomenological relaxation parameters and finite temperature in their theory. To compare our values with these more recent theoretical predictions, we refer to Table I. The predictions for chemical potential $|\mu| = 0.3$ eV, presented in Fig. 4 of Ref. [5], show higher values of $\mathrm{Re}[\sigma^{(3)}]$ than ours, with a discrepancy varying from one to two orders of magnitude depending on the phenomenological relaxation parameter introduced in the theory. Predictions from Ref. [7] for the same parameters agree with those of Cheng and co-workers [5]. Finally, in Ref. [15], theoretical values are compared to measurements performed with FWM on chip in a continuous regime. The theoretical values of the third-order surface conductivity are estimated to be around 10^{-18} $\mathrm{A\,m^2/V^3}$, three orders of magnitude higher than our values (Table I), while the experimental values are around 10^{-19} $\mathrm{A\,m^2/V^3}$, in better agreement with our results. The high discrepancy between the experimental results can be due to many factors, such as the continuous regime and the waveguiding geometry.

To conclude this discussion, it is clear that the values that we measure match the values reported in other experimental works better than those reported in theoretical studies. Possible explanations of these differences between theory and experiments are discussed in Ref. [5].

B. Out-of-plane components

To verify the theoretical assumption that the out-of-plane components of the susceptibilities can be neglected [5], we should considering working with sheet currents, with the problem that textbook expressions do not allow us to calculate the impact of the out-of-plane components, and therefore they limit the possibility to measure them; alternatively, we could use a 3D theory that neglects the local field and relates microscopic parameters to light propagation in a homogeneous medium. We have shown how to circumvent this problem to measure the out-of-plane components, and we show that $\chi_{xzxz} + \chi_{xzzx}$ and $\chi_{zxzz} + \chi_{zxxz}$ are negligible.

C. Temporal response

Measuring χ_{xxxx} is possible with one-beam techniques involving a single polarization. However, it does not offer the possibility to separate different contributions with different time responses. The 2D-OHD-OKE method allows us to record the temporal response of $\chi_{xyxy} + \chi_{xyyx}$ and χ_{xxyy} separately.

D. 3D versus 2D material parameters

Nonlinear optical properties are usually measured through amplitude changes, which have their origin in phase changes. Going from amplitude and phase variations to tensor components requires the use of a model. In this paper, we provide a complete analytical model from Maxwell's equation to the measured power (23). This expression differs from the one used in a bulk material. Therefore, we should refrain from using equations relating experimental phase changes to 3D propagation parameters in order to estimate the susceptibilities. Doing so would, for example, introduce the refractive index of the 2D material under consideration, while the expressions based on the current sheets would not. Indeed, our results show the possibility to measure the third-order surface susceptibilities (or the associated conductivities) considered in theoretical works [4,7], without estimating the refractive index of the 2D material.

V. CONCLUSION

To verify that the out-of-plane components of the third-order nonlinear optical susceptibility of graphene are negligible, we have developed the 2D-OHD-OKE method, and an appropriate model for the optical interaction of light at an interface with a 2D material. Six new values for the real and imaginary parts of these components for graphene have been provided at zero pump-probe delay, together with their time evolution. The out-of plane components that we measured are negligible.

We have shown that $\chi_{xyxy} + \chi_{xyyx}$ accounts for the fast birefringent and dichroic contribution to the nonlinear response, in agreement with [22] for the dichroic response. We have compared its magnitude with χ_{xxyy}, which has a slower (ps) relaxation time.

Equation (23) allows us to calculate the intrinsic parameters from the experimental data of 2D-OHD-OKE. It reveals the importance of taking the substrate into account, as it modifies the symmetric surface field. Our modeling can be used to discriminate between the optical and chemical interactions between a 2D material and its substrate. It could also help in the development of numerical simulation tools using sheet currents to model the nonlinear optical response of graphene. The 2D-OHD-OKE method presented here should apply to all 2D materials, and provide an efficient means to retrieve experimentally their fundamental parameters.

ACKNOWLEDGMENTS

This work is partially supported by the Belgian Federal Science Policy Office (BELSPO) under Grant No. IAP7-35. E.D. is funded by the Fund for Research Training in Industry and Agriculture (FRIA, Belgium).

[1] S. L. Yu, X. Q. Wu, Y. P. Wang, X. Guo, and L. M. Tong, Adv. Mater. **29**, 1606128 (2017).
[2] S. A. Mikhailov and K. Ziegler, J. Phys.: Condens. Matter **20**, 384204 (2008).
[3] K. J. A. Ooi, L. K. Ang, and D. T. H. Tan, Appl. Phys. Lett. **105**, 111110 (2014).
[4] J. L. Cheng, N. Vermeulen, and J. E. Sipe, New J. Phys. **16**, 053014 (2014).
[5] J. L. Cheng, N. Vermeulen, and J. E. Sipe, Phys. Rev. B **91**, 235320 (2015).
[6] B. Semnani, A. H. Majedi, and S. Safavi-Naeini, J. Opt. **18**, 035402 (2016).
[7] S. A. Mikhailov, Phys. Rev. B **93**, 085403 (2016).
[8] S. A. Mikhailov, Phys. Rev. B **95**, 085432 (2017).
[9] E. Hendry, P. J. Hale, J. Moger, A. K. Savchenko, and S. A. Mikhailov, Phys. Rev. Lett. **105**, 097401 (2010).
[10] S.-Y. Hong, J. I. Dadap, N. Petrone, P.-C. Yeh, J. Hone, and R. M. Osgood, Phys. Rev. X **3**, 021014 (2013).
[11] H. Zhang, S. Virally, Q. Bao, L. Kian Ping, S. Massar, N. Godbout, and P. Kockaert, Opt. Lett. **37**, 1856 (2012).
[12] W. Chen, G. Wang, S. Qin, C. Wang, J. Fang, J. Qi, X. Zhang, L. Wang, H. Jia, and S. Chang, AIP Adv. **3**, 042123 (2013).
[13] G. Demetriou, H. T. Bookey, F. Biancalana, E. Abraham, Y. Wang, W. Ji, and A. K. Kar, Opt. Express **24**, 13033 (2016).
[14] E. Dremetsika, B. Dlubak, S.-P. Gorza, C. Ciret, M.-B. Martin, S. Hofmann, P. Seneor, D. Dolfi, S. Massar, P. Emplit *et al.*, Opt. Lett. **41**, 3281 (2016).
[15] K. Alexander, N. A. Savostianova, S. A. Mikhailov, B. Kuyken, and D. Van Thourhout, ACS Photon. Article ASAP, doi:10.1021/acsphotonics.7b00559.
[16] R. I. Woodward, R. T. Murray, C. F. Phelan, R. E. P. d. Oliveira, T. H. Runcorn, E. J. R. Kelleher, S. Li, E. C. d. Oliveira, G. J. M. Fechine, G. Eda *et al.*, 2D Mater. **4**, 011006 (2017).
[17] C. Torres-Torres, N. Perea-López, A. L. Elías, H. R. Gutiérrez, D. A. Cullen, Ayse Berkdemir, F. López-Urías, H. Terrones, and M. Terrones, 2D Mater. **3**, 021005 (2016).
[18] Z. Lin, A. McCreary, N. Briggs, S. Subramanian, K. Zhang, Y. Sun, X. Li, N. J. Borys, H. Yuan, S. K. Fullerton-Shirey *et al.*, 2D Mater. **3**, 042001 (2016).

[19] T. Stauber, N. M. R. Peres, and A. K. Geim, Phys. Rev. B **78**, 085432 (2008).
[20] J. E. Sipe, J. Opt. Soc. Am. B **4**, 481 (1987).
[21] B. U. Felderhof and G. Marowsky, Appl. Phys. B **44**, 11 (1987).
[22] M. Mittendorff, T. Winzer, E. Malic, A. Knorr, C. Berger, W. A. de Heer, H. Schneider, M. Helm, and S. Winnerl, Nano Lett. **14**, 1504 (2014).
[23] X.-Q. Yan, J. Yao, Z.-B. Liu, X. Zhao, X.-D. Chen, C. Gao, W. Xin, Y. Chen, and J.-G. Tian, Phys. Rev. B **90**, 134308 (2014).
[24] N. A. Smith and S. R. Meech, Int. Rev. Phys. Chem. **21**, 75 (2002).
[25] M. Born, *Principles of Optics* (Cambridge University Press, Cambridge, 1999).
[26] P. Tassin, T. Koschny, and C. M. Soukoulis, Physica B **407**, 4062 (2012).
[27] R. W. Boyd, Z. Shi, and I. D. Leon, Opt. Commun. **326**, 74 (2014).
[28] R. A. Farrer, B. J. Loughnane, and J. T. Fourkas, J. Phys. Chem. A **101**, 4005 (1997).
[29] M. Currie, J. D. Caldwell, F. J. Bezares, J. Robinson, T. Anderson, H. Chun, and M. Tadjer, Appl. Phys. Lett. **99**, 211909 (2011).
[30] M. Breusing, S. Kuehn, T. Winzer, E. Malic, F. Milde, N. Severin, J. P. Rabe, C. Ropers, A. Knorr, and T. Elsaesser, Phys. Rev. B **83**, 153410 (2011).
[31] N. Vermeulen, D. Castelló-Lurbe, J. L. Cheng, I. Pasternak, A. Krajewska, T. Ciuk, W. Strupinski, H. Thienpont, and J. Van Erps, Phys. Rev. Appl. **6**, 044006 (2016).